Proceedings of the ASME 2015 International Technical Conference and Exhibition on Packaging and Integration of Electronic and Photonic Microsystems and ASME 2015 12th International Conference on Nanochannels, Microchannels, and Minichannels InterPACKICNMM2015

July 6-9, 2015, San Francisco, USA

InterPACKICNMM2015-48122

NUMERICAL SIMULATION OF ADVANCED MONOLITHIC MICROCOOLER DESIGNS FOR HIGH HEAT FLUX MICROELECTRONICS

Sebastian Scholl*
*Stanford University
Department of Mechanical Engineering
NanoHeat Laboratory
440 Escondido Mall Building 530
Stanford, California 94305 - USA
Email: sebastian.scholl@vki.ac.be

Catherine Gorle†
Farzad Houshmand
Tanya Liu
Hyoungsoon Lee
Yoonjin Won
Mehdi Asheghi
Kenneth Goodson
Stanford University
Department of Mechanical Engineering
NanoHeat Laboratory
440 Escondido Mall Building 530
Stanford, California 94305 - USA

Hooman Kazemi
Nuvotronics LLC
7586 Old Peppers Ferry Loop
Radford, VA 24141 - USA

ABSTRACT

This study considers CFD simulations with conjugate heat transfer performed in the framework of designing a complex micro-scale cooling geometry. The numerical investigation of the three-dimensional, laminar flow (Reynolds number smaller than 480) and the solid conduction is done on a reduced model of the heat sink micro-structure to enable exploring a variety of configurations at a limited computational cost. The reduced model represents a unit-cell, and uses periodic and symmetry boundary conditions to mimic the conditions in the entire cooling manifold. A simulation of the entire heat sink micro-structure was performed to verify the unit-cell set-up, and the comparison demonstrated that the unit-cell simulations allow reducing the computational cost by two orders of magnitude while retaining accurate results. The baseline design for the unit-cell represents a configuration used in traditional electronic heat sinks, i.e. a simple channel geometry with a rectangular cross section, with a diameter of 50 μm, where the fluid flows between two cooling fins. Subsequently three types of modified geometries with feature sizes of 50 μm were considered: baffled geometries that guide the flow towards the hotspot region, geometries where the fins are connected by crossbars, and a woodpile structure without cooling fins. Three different mass-flow rates were tested. Based on the medium mass-flow rate considered, the woodpile geometry showed the highest heat transfer coefficient with an increase of 70% compared to the baseline geometry, but at the cost of increasing the pressure drop by more than 300%. The crossbar geometries were shown to be promising configurations, with increases in the heat transfer coefficient of more than 20% for a 70% increase in pressure drop. The potential for further optimization of the crossbar configurations by adding

*Corresponding author, visiting researcher at Stanford University. Permanent address: Von Karman Institute for Fluid Dynamics, Chaussée de Waterloo 72, 1640 Rhode-Saint-Gènese - Belgium.
† Current affiliation: Department of Civil Engineering and Engineering Mechanics, Columbia University, New York, NY, 10027

or removing individual crossbars will be investigated in a follow up study. The results presented demonstrate the increase in performance that can be obtained by investigating a variety of designs for single phase cooling devices using unit-cell conjugate heat transfer simulations.

NOMENCLATURE

Roman

c_p iso-baric specific heat capacity ..... $[J/kgK]$
D_h hydraulic diameter ..... $[m]$
htc heat transfer coefficient ..... $[Wm^{-2}K]$
k thermal conductivity ..... $[Wm^{-1}K^{-1}]$
P pressure ..... $[kg/ms^2]$
q heat flux under the solid slab ..... $[W/m^2]$
q_w wall heat flux at the interface ..... $[W/m^2]$
T temperature ..... $[K]$
u velocity ..... $[m/s]$
U_∞ bulk velocity ..... $[m/s]$
x, y, z Cartesian coordinates ..... $[m]$

Greek

ρ density ..... $[kg^1m^{-3}]$
μ dynamic viscosity ..... $[Pa^1s^1]$
ij Einstein'sche summation convention

Acronyms

CFD Computational Fluid Dynamics
CHT Conjugate Heat Transfer
GaN Gallium nitride
SiC Silicon Carbide
SIMPLE Semi Implicit Pressure Linked Equations
TIM Thermal Interface Material

Super- and Subscripts

f fluid
s solid
w wall quantity
∞ free stream quantity

INTRODUCTION

Increasing integration density of electronic components and chip power dissipation are driving the development of innovative thermal design strategies, since traditional cooling techniques cannot meet the thermal management requirements. Integral liquid cooling, where the on-chip heat generation sites are cooled directly to extract the dissipated heat with microfluidic flow through the chip or package, could overcome these limitations. [1] [2]

The first design for microchannel heat sinks was proposed by Tuckerman and Pease [3], and consisted of microchannels running parallel to a heat-base. Since then, this conventional configuration has been further investigated [4] and significant efforts have been made to enhance the design [5].

The PolyStrata® manufacturing process developed by Nuvotronics[1] offers new opportunities for fabricating monolithic, complex micro-scale structures [6], allowing arbitrary combinations of a permanent polymer with fabrication tolerances of micrometers. This process enables the fabrication of very complex micro-scale geometries, opening up an immense design space.

This manufacturing technique creates a significant potential for designing a new variety of geometrical configurations that could improve the performance of the heat sinks.

Heat transfer augmentation devices, i.e. fins, woodpile structures, fins with connecting cross-bar and other enhanced features can be used to improve the efficiency of the micro-scale heat sink. Computational tools can aid significantly in the process of investigating the large number of potential geometrical configurations for the heat sink micro-structure. Similar studies for larger scale devices such as turbomachinery cooling channels have demonstrated the potential of using CFD simulations to evaluate the performance of different designs. [7].

The present study presents CFD simulations with conjugate heat transfer of different geometrical designs for a complex micro-scale heat sink. The simulations are performed for a reduced model of the entire heat sink micro-structure to enable exploring a variety of configurations at a limited computational cost. The reduced model represents a unit-cell and uses periodic and symmetry boundary conditions to mimic the conditions in the entire cooling manifold.

The baseline configuration is a channel with copper fins. The enhanced geometries include: (a) five configurations where baffles are added between the copper fins to guide the flow, (b) one configuration where crossbars connect the copper fins, (c) a woodpile structure that consists of stacked bars. The objective of the CFD simulations is to identify which designs provide an improved heat transfer performance for an acceptable increase in pressure drop. Moreover, the typology (baffles, crossbars or woodpile) with the most promising capabilities for further optimization will be identified. The following section describes the computational model for the geometries considered, including a description of the geometries and material properties, the governing equations, boundary conditions and the numerical solution method. The results section first presents the output quantities of interest and a thorough grid depen-

[1] www.nuvotronics.com

dency study. In addition, the use of the reduced model with periodic boundary conditions is justified by comparing the results to simulation results of the full geometry. Finally, results for the various channel designs are presented and the design configurations that will be considered for further optimization in a follow up study are identified.

DESCRIPTION OF COMPUTATIONAL MODEL

Geometry description and material properties

Figure 1 sows the baseline geometry, which consists of two cooling fins that define an empty channel with a rectangular cross section and a hydraulic diameter of 100 μm. The channel and the copper fins are 460 μm long, the fins are 300 μm high. An inlet and an outlet section of 200μm and 300 μm length , respectively, have been added to the computational domain to avoid influencing the flow through the channel by the inlet or outlet boundary conditions.
The heat is distributed from the gates in the GaN layer (See Fig. 1) with a surface of 2x160 μm through the SiC layer with a thickness of 100μm and the stress relieving TIM and epotek layers with respective thicknesses of 4 and 10 μm. The epotek layer is in contact with the coolant and the heat dissipating copper fins. The working fluid is water. The fluid and solid properties are summarized in Table 2.
Figure 2 shows sketches of the variations on the baseline geometry (2(a)), where additional features, such as cross bars (see Fig. 2(b)), baffles (see Fig. 2(c)-(e)) and woodpiles (see Fig. 2(f)), were added to redirect flow and increase the heat transfer. The overall dimensions of these geometries are identical to those of the baseline configuration.
The squared crossbars, 50x50μm are bars connecting the cooling fins to increase the cooling surface area and to accelerate and redirect the flow towards the hotspot. The baffles were placed at the inlet and outlet sections, increasing the path for each flow particle and also used to redirect the flow towards the hotspot. The woodpile structure lacks cooling fins, but consists of cross bars that are stacked perpendicularly in the entire single cell domain. In addition to the three baffled geometries shown in Fig. 2, two more configurations were considered, which are not detailed in this paper due to their similarity of the baffled configurations 4 and 5. The woodpile structure has the largest surface area (see table 1) and thus providing a high potential for increasing the heat transfer.

Governing Equations

Previous studies have demonstrated that the macrosclae Navier-Stokes equations and energy equations sufficiently describe the flow and heat transfer in microchannel heat sinks [8] [9] [10] [11]. The fluid flow and

TABLE 2: MATERIAL PROPERTIES.

material	conductivity [W/mK]
GaN	$-0.1623T+214.17$
SiC	$0.0038T^2-4.1734T+1259$
TIM	314
epotek	30
copper	387.6
water	0.6

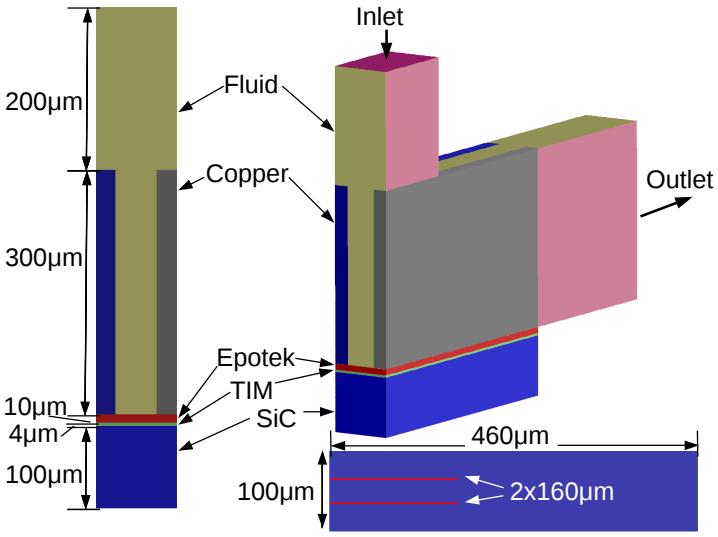

FIGURE 1: GEOMETRY OF SINGLE CELL MODEL.

the heat transfer in the fluid and solid domain are therefore governed by the following equations [12]:
• the continuity equation:

$$\frac{\partial}{\partial x_j}(\rho u_j) = 0, \tag{1}$$

• the momentum equation:

$$\frac{\partial}{\partial x_j}(\rho u_j u_j) = -\frac{\partial P}{\partial x_i} + \frac{\partial}{\partial x_j}\left(\mu_f \frac{\partial u_i}{\partial x_j}\right), \tag{2}$$

• the energy equation for the fluid domain:

$$\frac{\partial}{\partial x_j}(\rho u_j C_p T_f) = \frac{\partial}{\partial x_j}\left(k_f \frac{\partial T_f}{\partial x_j}\right), \tag{3}$$

TABLE 1: EXTRA SURFACE AREA.

geometry	baseline	baffled	crossbar	woodpile
surface area	$3.22 \times 10^{-8} m^2$	$3.07 - 3.22 \times 10^{-8} m^2$	$3.22 - 3.49 \times 10^{-8} m^2$	$4.085 \times 10^{-8} m^2$
difference compared to baseline	-	-5 - 0 %	0 - 8.4%	27%

• the energy equation for the solid domain:

$$0 = \frac{\partial}{\partial x_j}\left(k_s \frac{\partial T_s}{\partial x_j}\right). \quad (4)$$

Boundary Conditions

A constant heat flux was prescribed at the bottom of the solid on the two gates (Fig. 1). Two different heat fluxes, corresponding to two different powers were considered: with 1.97×10^9 and $2.46 \times 10^9 W/m^2$. All other solid outer walls were assumed to be adiabatic. In the fluid domain, no-slip conditions were applied on the interfaces to the solid domain and on the fluid top boundary. A coupled wall boundary condition was used to compute the temperature at the solid-fluid interface walls. Dealing with a steady state problem in fluid and solid domain, the conjugate heat transfer was solved with a monolithic coupling approach as provided by the ANSYS Fluent software, thus assuring continuity of temperatures and heat fluxes at the fluid-solid interfaces:

$$T_s = T_f, \quad (5)$$

$$k_s \left(\frac{\partial T_s}{\partial n}\right) = k_f \left(\frac{\partial T_f}{\partial n}\right). \quad (6)$$

Symmetry boundary conditions were applied on the front and the inlet and outlet region side walls (see Fig. 1). A constant pressure outlet condition was applied on the outlet. The mass-flow at the inlet was varied from 1.889 to 7.556×10^{-5} kg/s and the inlet temperature was set to 343K (Table 3).

Solver

The numerical simulations solved the incompressible three-dimensional steady-state laminar flow and the conjugate heat transfer problem using the simulation software ANSYS Fluent 15.0.0 [13]. The code uses the finite volume method to solve the governing equations of fluid flow and heat transfer in the fluid and solid domain.The SIMPLE algorithm was employed to treat the coupling between the pressure and the velocities. All discretization schemes used were of second order.
The minimal convergence criterion was set to 10^{-5} for the continuity and momentum equation and to 10^{-8} for the energy equation.

TABLE 3: SIMULATION PARAMETERS.

parameter	value
single cell mass flow rate	$1.778 - 7.556 \times 10^{-5}$kg/s
single cell heat flux at the gate	2.46 W/cm2
Inlet temperature	343 K

RESULTS AND DISCUSSION

This section first presents the definition of the output quantities of interest. Subsequently the results of the grid dependency study are included and the comparison of the reduced single cell and full geometry results is presented to demonstrate the validity of the set-up of the computational model. Finally, the results for all geometrical configurations considered are presented to evaluate the performance of the different designs.

Output quantities of interest

The quantities used in the following sections are the temperature at the gate T_{max}, the temperature at the interface from solid to fluid T_w, the pressure drop from inlet to outlet of the fluid domain ΔP and the heat transfer coefficient htc. The heat transfer coefficient is a frequently used engineering parameter during the thermal design. It is derived from Newton's law of cooling:

$$q = h(T_w - T_\infty), \quad (7)$$

with the wall temperature T_w, the free-stream temperature T_∞, the heat flux q and the heat transfer coefficient h.

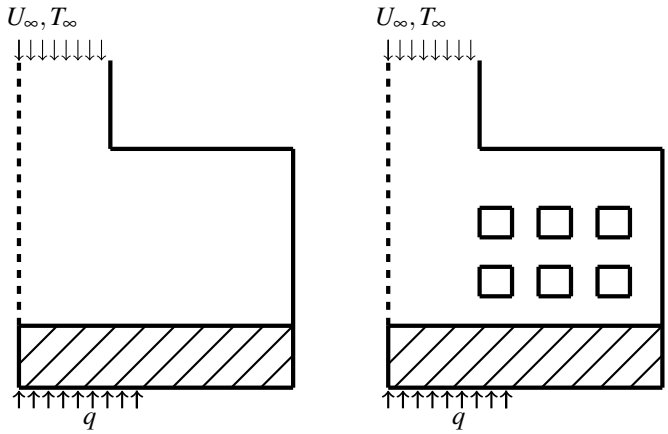

(a) Baseline configuration

(b) Crossbar configuration

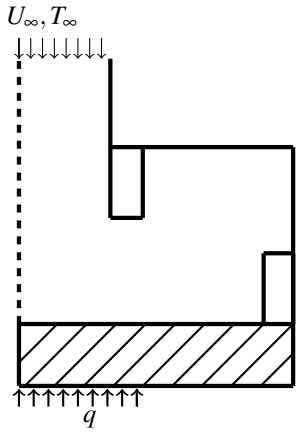

(c) Baffled 1 configuration

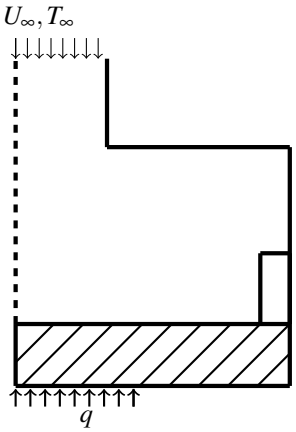

(d) Baffled 4 configuration

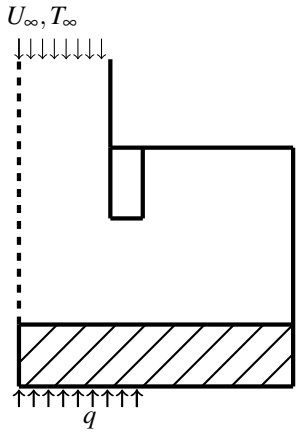

(e) Baffled 5 configuration

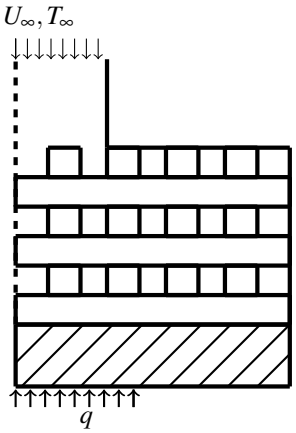

(f) Woodpile configurations

FIGURE 2: SKETCHES OF INVESTIGATED GEOMETRIES.

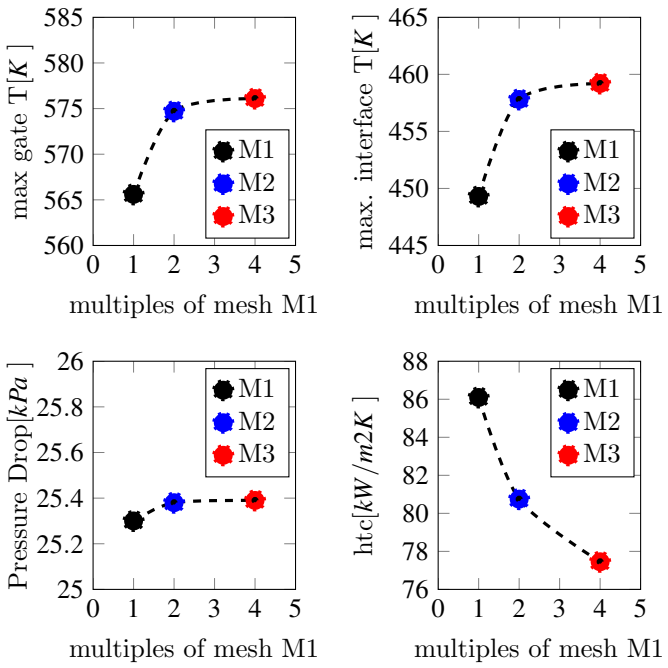

FIGURE 3: Mesh dependence study.

Mesh description and grid dependency study

A fully structured hexahedra mesh was constructed, using global and local size functions to adjust the mesh size as needed. Special care was taken to resolve the very thin solid layers, in particular the GaN surface where the heat flux was imposed. The smallest mesh, M1, contained one cell at this surface. Mesh M2 contained two and mesh M3 four cells. The grid influence on the solutions was checked on those three different meshes for the baseline geometry. Table 4 summarizes the mesh properties.

Figure 3 shows the values for the maximal temperature a the gates and for the pressure drop inside the channel obtained with the different meshes. While a significant change of the results from mesh M1 to mesh M2 is still visible, further increasing the mesh resolution does not change the results considerably. The temperature at the gate only changes by 0.3%, the pressure drop by even less than that with 0.005%. Only the heat transfer coefficient still changed slightly with around 4%. Figure 4 shows the temperature distribution at the fluid to solid interface (at the epotek layer) and the temperature distribution from fluid inlet along the copper fin down to the gate. Both temperature distributions confirm the grid independence from mesh M2 to mesh M3. Hence, to keep a balance between computational time and prediction accuracy mesh M2 was chosen for the following studies.

TABLE 4: MESH STUDY FOR BASELINE MODEL.

	M1	M2	M3
cells	0.18M	0.89M	6.56M
faces	0.60M	2.84M	20.36M
nodes	0.24M	1.05M	7.23M
gate cells	1	2	4
T_{gate} [K]	565.6	574.7	576.1
$T_{interface}$ [K]	449.3	457.8	459.2
ΔP [kPa]	25301	25380	25394
htc [W/m2K]	86095	80747	77453

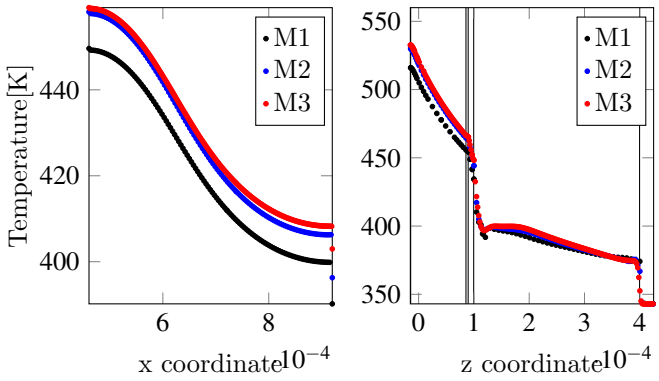

(a) Temperature at interface (b) Temperature along fin and through solid parts.

FIGURE 4: Temperature distribution dependent on the meshes.

Comparison with full device

In [14] a conjugate heat transfer CFD simulation of the full heat sink micro-structure was performed. Here, we compare these results with the single cell simulation results to justify the validity of simulating the reduced single cell model to represent the full device. The used solver was again ANSYS Fluent 15.0 and the used scheme a second order numerical scheme with a total mesh size of 8.1M cells. The mass flow is non-uniform in the heat sink. The mass flow rates through individual microchannels depend on the inlet and outlet locations and on the manifold design. Table 5 shows comparable values for the mass flow of single cells out of the full microchannel heat sink compared with single cell simulations. The corresponding pressure drops are in good agreement and hence indicate that the unit cell is a valid representation of the full device.

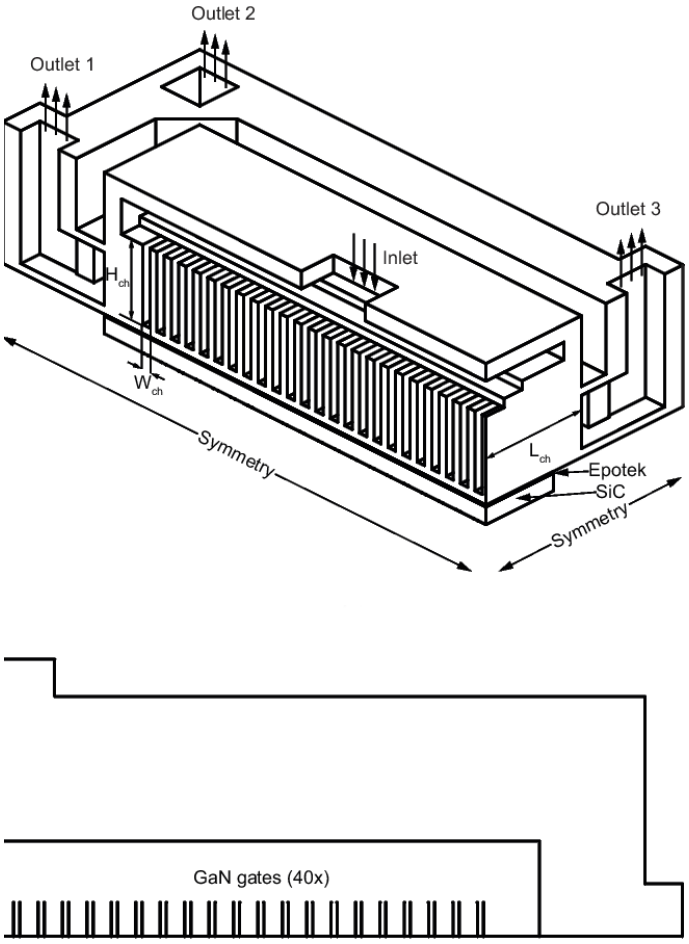

FIGURE 5: Geometry of full device model.

TABLE 5: PRESSURE DROP COMPARISON.

$\dot{m}$ full model	full model ΔP	$\dot{m}$ single cell	single cell ΔP
$1.95 \cdot 10^{-2} g/s$	$8.66 kPa$	$1.889 \cdot 10^{-2} g/s$	$7.34 kPa$
$3.83 \cdot 10^{-2} g/s$	$22.0 kPa$	$3.778 \cdot 10^{-2} g/s$	$25.4 kPa$
$7.54 \cdot 10^{-2} g/s$	$79.6 kPa$	$7.556 \cdot 10^{-2} g/s$	$94.0 kPa$

Analysis of the flow field for different configurations

Figure 8 shows velocity contour plots on a plane through the center of the channel for the different geometries considered. The basic geometry (Fig. 8(a)) shows the flow from inlet to outlet. Figure 8(c) shows how the flow field is modified in the presence of two baffles at the inlet and outlet section. The flow is redirected towards the hot spot, creating higher velocities near the interface, but also

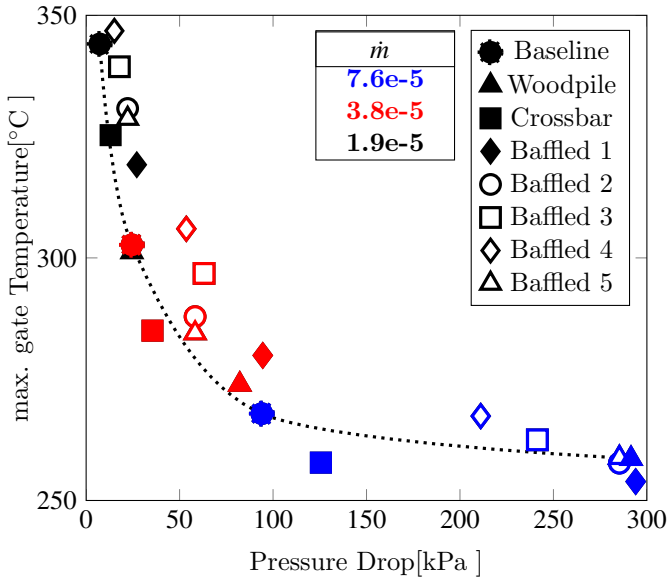

FIGURE 6: SIMULATION RESULTS FOR SIMULATED CONFIGURATIONS.

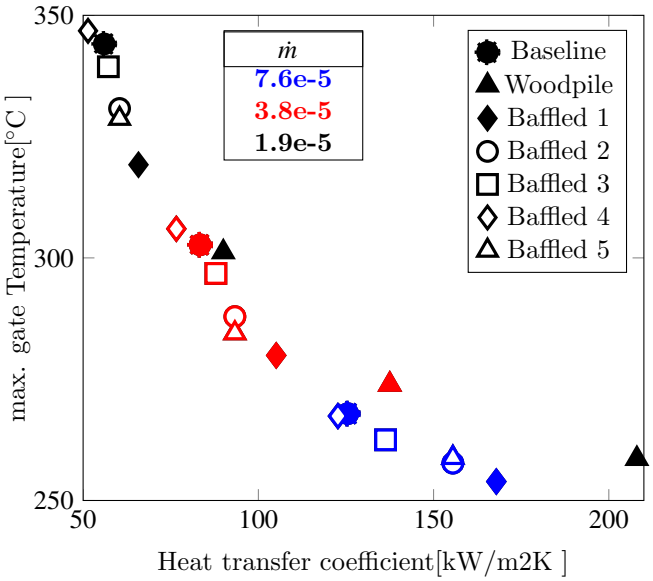

FIGURE 7: SIMULATION RESULTS FOR DIFFERENT CONFIGURATIONS SHOWING A NON-LINEAR DEPENDENCE OF THE TEMPERATURE ON THE HEAT TRANSFER COEFFICIENT.

near the corners of the baffles, with a velocity of 12m/s. Figure 8(d) shows the velocity contours of the geometry with the inlet baffle removed, highlighting the importance of the inlet baffle, since the redirection of the flow towards the hot spot is weaker in this case. Figure 8(e) shows the baffled case with the outlet baffle removed. Here, the velocity is only slightly increased and the flow even more directed towards the hotspot.
The woodpile and crossbar velocity contour plots indicate possible improvements on these geometries since in-between the bars, the flow is not well distributed. Nonetheless, the crossbar configuration shows again a redirection of the flow field toward the hotspot. The woodpile geometry has a totally different flow field, because the cooling fins have been replaced by bars in the center of the simulation domain.

Evaluation of heat transfer enhancement

Fig. 6 shows the temperature as a function of the pressure drop for the considered configurations. Each configuration was investigated for three different mass-flows. The baseline configuration shows the highest temperature, but also the lowest pressure drop. The crossbar and the woodpile configuration have a better performance in terms of heat transfer, but the pressure drop increases considerably, in particular for the woodpile geometry. Furthermore, as Fig. 8 shows, the maximal velocity in the channel increases from baseline configuration to the other configurations from 7.1m/s to 12.2 m/s.

The redistribution of the flow field affects the heat transfer between the fins. Figure 9 shows that the heat transfer coefficient increases with the added features. For instance, with the baffles at the inlet, the heat transfer coefficient increases not only locally at the baffle, but also closer to the hotspot. Furthermore the wetted area increases with added features as Table 1 summarizes.
Figure 7 demonstrates that an increasing heat transfer coefficient, either by a higher mass-flow or by adding feature to the geometry, decreases the temperature, but only to a certain extend. The decrease of the maximal gate temperature with increased heat transfer coefficient flattens out, if the heat transfer coefficient is increased.
Evaluating and comparing all tested configurations, the crossbar configuration provides a good trade-off between increased heat transfer and acceptable pressure losses among the tested configurations. This geometry also leaves room for further investigations and optimization due to the possibility to add or remove single crossbars, and to place them in different positions, which is presented in a follow-up study.

CONCLUSIONS

A numerical investigation of the three-dimensional flow and conjugate heat transfer has been performed for different geometrical designs of a complex micro-scale heat sink. The baseline geometry for the full heat sink consists of an in-

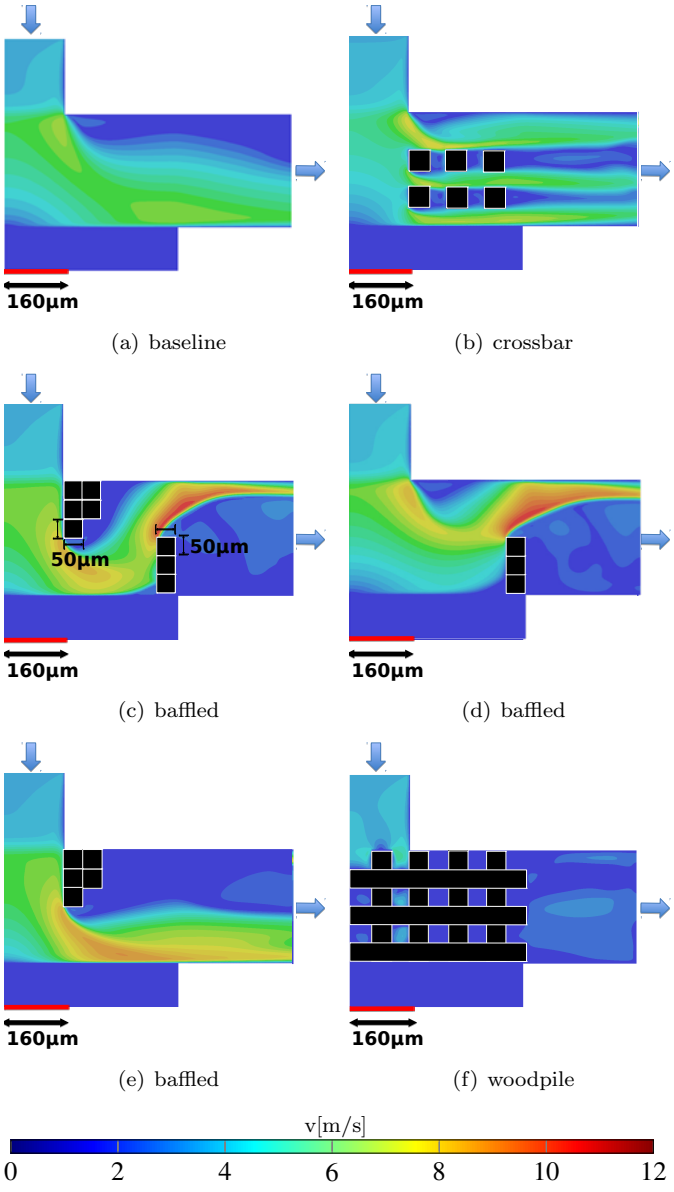

FIGURE 8: VELOCITY CONTOUR FOR VELOCITY OF DIFFERENT DESIGNS. CROSS SECTION AT SYMMETRY PLANE.

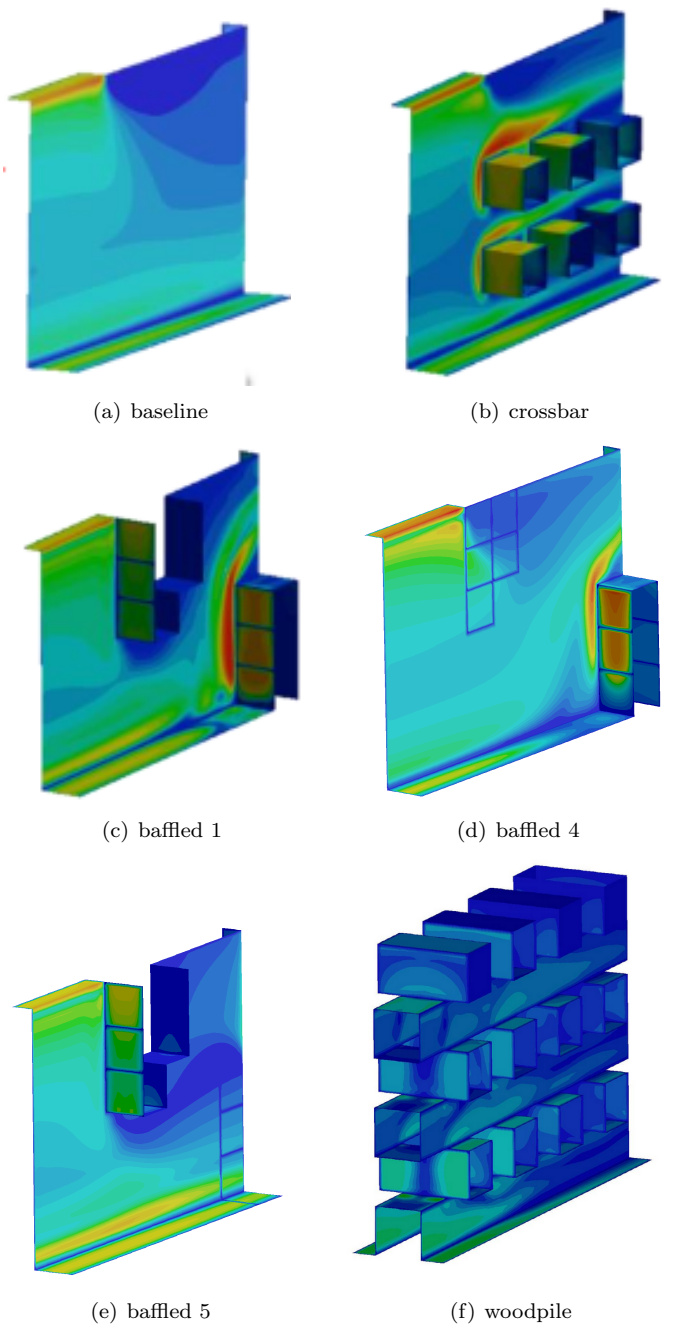

FIGURE 9: HEAT TRANSFER COEFFICIENTS OF DIFFERENT DESIGNS.

let manifold feeding fluid through 48 parallel channels with copper fins and an outlet manifold. The simulations were performed for a reduced model of the entire heat sink microstructure to enable exploring a variety of configurations at a limited computational cost. The reduced model represented a unit-cell (i.e., a single channel) and used periodic and symmetry boundary conditions to mimic the conditions in the entire cooling manifold. A comparison of the pressure drop obtained from the unit cell and the full device simulations was performed for the baseline design, showing a good agreement with differences in pressure drop of

around 15%. These differences are mainly caused by the manifold design in the full model, which results in a strong non-uniformity of the mass flow through the different channels. In addition to the baseline geometry different unit cell geometries have been simulated and compared regarding their cooling performance: The enhanced geometries included: (a) five configurations where baffles were added between the copper fins to guide the flow towards the hot spot (b) one configuration where crossbars connected the copper fins, and finally (c) a woodpile structure that consisted of stacked bars. Three different mass flow rates were simulated, and in all cases the use of enhanced geometrical features resulted in improved cooling performances and in an increase of the pressure drop. The woodpile geometry showed the highest increase in heat transfer, e.g., for the medium mass-flow rate considered it increased by 70%, but also the highest increase in the pressure drop (300%). The cooling configuration using crossbars to connect the existing cooling fins was found to be the optimal configuration in terms of increasing the heat transfer coefficient at an acceptable increase in pressure drop. This configuration also provides an opportunity for further optimization by modifying the number and the location of the crossbars in between the fins.

ACKNOWLEDGMENT

This project was supported in part by the U.S. Defense Advanced Research Projects Agency Microsystems Technology Office ICECool Applications Program under agreement number Nuvo-SFD-1401-1066. Disclaimer: The views, opinions, and/or findings contained in this article/presentation are those of the author/presenter and should not be interpreted as representing the official views or policies, either expressed or implied of the Defense Advanced Research Projects Agency or Department of Defense.

REFERENCES

[1] Bloschock, K., and Bar-Cohen, A., 2012. "Advanced thermal management technologies for defense electronics". *Proc. of SPIE Vol. 8405,.*

[2] Bar-Cohen, A., and Geisler, K., 2011. "Cooling for the electronic brain". *Mechanical Engineering, pp.38-41.*

[3] Tuckerman, D., and Pease, R., 1981. "High performance heat sinking for vlsi". *IEEE Electron Device Lett. 2, 126-129.*

[4] Garimella, S., and Harichian, T., 2013. "Microchannel heat sinks for eelectronic cooling". *The Encyclopedia of Thermal Packaging vol. 1.*

[5] P.S.Lee, and Garimella, S., 2006. "Thcooling developing flow and heat transfer in rectangular mmicrochannel of different aspect ratios". *International Journal of Heat and Mass Transfer.*

[6] Popovic, Z., Rondineau, S., Filipovic, D., Sherrer, D., Nichols, C., Rollin, J., and Vanhille, K., 2008. "An enabling new 3d architecture for microwave components and systems-introduction to a manufacturing technology dedesign to produce 3d miniature circuit components.". *Microwave Journal.*

[7] Xie, G., Sunden, B., and Zhang, W., 2011. "Comparison of pins/dimples/ protrusions cooling concepts for a turbine blade tip-wall at high reynolds numbers". *ASME Journal of Heat Transfer.*

[8] Fedorov, A., and Viskanta, R., 2000. "Three-dimensional conjugate heat transfer in the microchannel heat sink for electronic packaging". *International Journal of Heat and Mass Transfer.*

[9] Qu, W., and Mudawar, I., 2002. "Experimental and numerical study of pressure drop and heat transfer in a single-phase micro-channel heat sink". *International Journal of Heat and Fluid Flow.*

[10] Judy, J., Maynes, D., and Webb, B., 2002. "Characerization of frictional pressure drop for liquid flows through microchannels". *International Journal of Heat and Mass Transfer.*

[11] Gamriat, G., Favre-Marinet, M., and Asendrych, D., 2005. "Conduction and entrance effects on laminar liquid flow and heat transfer in rectangular microchannels". *International Journal of Heat and Mass Transfer.*

[12] Incopera, F., and Witt, D. D., 2007. *Fundamentals of Heat and Mass Transfer.* John Wiley and Sons.

[13] *ANSYS Fluent User's Guide, Release 15.0, November 2013.*

[14] Unpublished, Liu, T. L., Houshmand, F., Gorle, C., Lee, H., Won, Y., Scholl, S., Ashegi, M., Goodson, K., and Kazemi, H., 2015. Full scale simulation of an integrated monolithic heat sink for thermal management of a high power density gan chip.